EPR analysis of imidazole binding to **Methanosarcina acetivorans** protoglobin

Reference:

Van Doorslaer Sabine, van den Bosch Martje, Tilleman Lesley, Dewilde Sylvia.- EPR analysis of imidazole binding to **Methanosarcina acetivorans** protoglobin

Applied magnetic resonance - ISSN 0937-9347 - 46:4(2015), p. 421-433

DOI: http://dx.doi.org/doi:10.1007/s00723-014-0638-z

EPR Analysis of Imidazole Binding to Methanosarcina acetivorans *Protoglobin*

Sabine Van Doorslaer, Martje van den Bosch, Lesley Tilleman & Sylvia Dewilde

Applied Magnetic Resonance

ISSN 0937-9347
Volume 46
Number 4

Appl Magn Reson (2015) 46:421-433
DOI 10.1007/s00723-014-0638-z

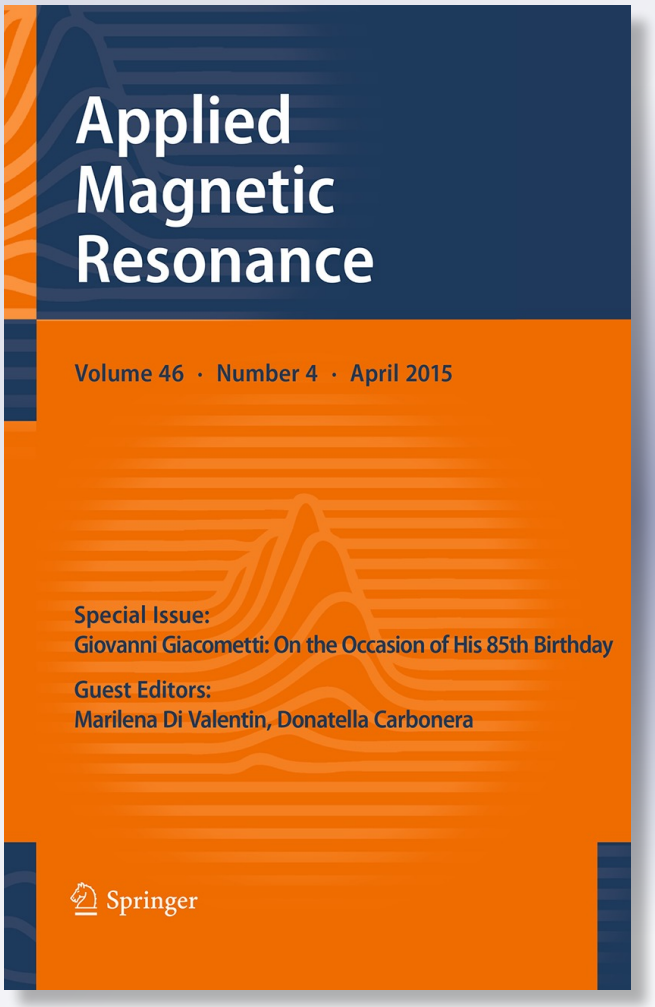

Springer

Appl Magn Reson (2015) 46:421–433
DOI 10.1007/s00723-014-0638-z

Applied
Magnetic Resonance

EPR Analysis of Imidazole Binding to *Methanosarcina acetivorans* Protoglobin

Sabine Van Doorslaer · Martje van den Bosch · Lesley Tilleman · Sylvia Dewilde

Received: 7 October 2014 / Revised: 3 December 2014 / Published online: 9 January 2015

Abstract Protoglobins form an unusual class of globin proteins with surprising structural features, such as a highly ruffled heme. Electron paramagnetic resonance spectra of the frozen solution of the ferric imidazole complex of *Methanosarcina acetivorans* protoglobin reveal the existence of two low-spin ferric heme complexes. Hyperfine sublevel correlation spectroscopy was used to study the imidazole complex of this protoglobin as well as the imidazole complex of horse heart myoglobin for comparison. The spin Hamiltonian values obtained for the dominant contribution of the imidazole-ligated protoglobin agree with a heme conformation in which the plane of the exogenous imidazole is turned more than 30° versus the imidazole plane of the proximal histidine ligand. In turn, the electron paramagnetic resonance data of the minority complex indicate a second conformer, in which the two ligand planes are aligned almost parallel to each other with a lengthened iron–nitrogen bond for the exogenous imidazole ligand.

This paper is in honor of Giovanni Giacometti on the occasion of his 85th birthday.

Electronic supplementary material The online version of this article (doi:10.1007/s00723-014-0638-z) contains supplementary material, which is available to authorized users.

S. Van Doorslaer (✉) · M. van den Bosch
BIMEF Laboratory, Department of Physics, University of Antwerp, Universiteitsplein 1, 2610 Antwerp, Belgium
e-mail: sabine.vandoorslaer@uantwerpen.be

L. Tilleman · S. Dewilde
PPES Laboratory, Department of Biomedical Sciences, University of Antwerp, Universiteitsplein 1, 2610 Antwerp, Belgium

1 Introduction

Within the globin superfamily, protoglobin (Pgb) has surprising structural features. These single-domain archaeal heme proteins have been related to globin-coupled sensors [1]. Several Pgbs have by now been identified in *Archaea* and *Bacteria* [1–4], of which only two have been characterized, namely the one from the obligate aerobic hyperthermophile *Aeropyrum pernix* [3] and from the strictly anaerobic methanogen *Methanosarcina acetivorans* [3, 5]. The presence of a globin, which can be related with O_2 metabolism, is very surprising in the latter anaerobic methanogen. The versatile *Methanosarcina* can exploit acetate, methanol, CO_2 and CO as carbon sources for methanogenesis [6]. Pgb may play a yet unknown role in the CO metabolism of these archaeal organisms.

Up till now, a crystal structure is available only for different mutants of the homodimeric protoglobin of *M. acetivorans*, referred to hereafter as *Ma*Pgb [5, 7, 8]. The structure of the oxygenated ferrous form of *Ma*Pgb* (the asterisk indicates the Cys(E20)101 → Ser mutation) revealed many unusual structural aspects [5]. First of all, the heme group is highly distorted and completely buried in the protein matrix by a number of Pgb-specific loops, including a 20 amino-acid long N-terminal loop. In contrast to the mammalian myoglobins (Mb) with a globin fold of eight helices (named helices A–H), the oxygenated ferrous *Ma*Pgb* fold has nine helices (Z, A, B, C, E, F, G, H and H′). Furthermore, two apolar tunnels govern the access of exogeneous ligands to the heme group. While many globins have a His at position 7 of the E helix that stabilizes the exogeneous ligands, this is a Val in the case of *Ma*Pgb*. In addition to small gas molecules, such as O_2, NO and CO, MaPgb* can bind in vitro cyanide, azide, and even bulky ligands, such as imidazole (Im) and nicotinamide [7, 8]. In all binding cases, the heme is distorted (highly ruffled). Moreover, the heme distal site of Pgb seems to reshape in a ligand-

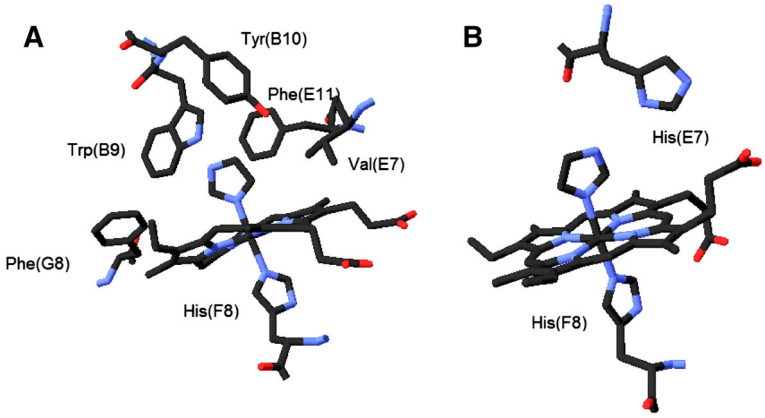

Fig. 1 Heme site of (**a**) imidazole-ligated ferric MaPgb* [structure from PDB bank (3ZJP) 1.38 Å resolution] and (**b**) imidazole-ligated ferric swMb [structure from PDB bank (1MBI) 2.0 Å resolution]. A number of important amino-acid residues of the heme pocket are *highlighted*

dependent way, with Phe(E11)93 acting as a ligand sensor, controlling heme accessibility via the tunnel system by changing the conformation of Trp(B9)60 [8].

Figure 1 shows a comparison between the heme environment of imidazole-ligated ferric *Ma*Pgb* (*Ma*Pgb*Im) [8] and of imidazole-ligated ferric sperm whale Mb (swMbIm) [9]. In both cases, the imidazole ligand adopts an orientation slightly tilted versus the (average) heme plane (~15°). Furthermore, the conserved proximal His at position F8 is almost eclipsing with one of the $N_{pyrrole}$–Fe–$N_{pyrrole}$ axes, and the plane of the imidazole is staggered relative to the heme pyrrole nitrogen atoms. One of the big differences between the two structures lies in the heme ruffling: swMbIm has a relatively flat heme, while the heme is strongly ruffled in the case of *Ma*Pgb*Im. Furthermore, the orientation of the imidazole in swMbIm is mainly dictated by the coordination to the heme and the hydrogen bonding between the imidazole ligand and the His residue at position E7. In *Ma*Pgb*Im, the imidazole ligand is stabilized mainly by Tyr(B10)61 and Trp(B9)60, with several van der Waals contacts with the hydrophobic heme distal site residues, such as Val(E7)89 and Phe(G7)145.

Electron paramagnetic resonance (EPR) revealed a strong influence of the heme ruffling on the electronic structure (and thus EPR signature) of cyanide-ligated ferric MaPgb* [10]. Furthermore, deletion of the 20 amino-acid long N-terminal loop or mutation of Phe(G7)145 → Trp leads to a clear change in the principal *g* values of the corresponding complex with cyanide. The EPR observation upon the loop deletion confirms the stabilization of the heme propionate groups by the N-terminal loop as observed in all X-ray structures of MaPgb* variants [5, 7, 8]. Furthermore, the EPR results imply that Phe(G7)145 has an influence on the orientation of the cyanide ligand. In the present study, we use EPR to investigate how the electronic structure of *Ma*Pgb*Im and of imidazole-ligated horse heart Mb (hhMbIm) compare.

2 Materials and Methods

2.1 Sample Preparation

The protoglobin mutant bearing the Cys(E20)101 → Ser substitution will be referred to as *Ma*Pgb* in this paper. The recombinant expression and purification was performed as described previously [10]. The protein was dissolved in a 50 mM Tris-HCl buffer, pH 8.5. Ferric hhMb was purchased from Sigma-Aldrich as lyophilized powder. The powder was dissolved in a 50 mM Tris-HCl buffer at pH 7.5. A 10-fold excess of imidazole (Sigma-Aldrich) was added to the proteins to form the imidazole-ligated forms. The final concentrations were 1 mM hhMbIm and ~0.4 mM *Ma*Pgb*Im.

2.2 EPR Spectroscopy

The X-band continuous wave (CW) EPR experiments were performed on a Bruker ESP300E spectrometer [microwave (mw) frequency ~9.44 GHz] equipped with a

liquid-Helium cryostat (Oxford Inc.). The EPR spectra were taken with a modulation amplitude of 0.5 mT and a modulation frequency of 100 kHz. The microwave power was 5 mW. The temperatures at which the spectra were recorded are given in the figure captions.

Pulsed EPR experiments were performed on a Bruker Elexsys E580 spectrometer (mw frequency of 9.76 GHz) equipped with a liquid-helium cryostat (Oxford Inc.). All experiments were performed at 5 K.

For the two-dimensional ESE (electron spin echo)-detected EPR spectrum, a $\pi/2$–τ–π–τ–echo pulse sequence was used with $t_{\pi/2} = 16$ ns, $t_{\pi} = 32$ ns, and the interpulse distance τ being varied from 96 to 2,136 ns in steps of 8 ns.

The HYSCORE (hyperfine sublevel correlation spectroscopy) experiments [11] were performed using the $\pi/2$–τ–$\pi/2$–t_1–π–t_2–$\pi/2$–τ–echo sequence with pulse lengths $t_{\pi/2} = 16$ ns, $t_{\pi} = 32$ ns. The times t_1 and t_2 were varied from 96 to 4,880 ns in steps of 16 ns. Experiments were performed for different τ values as specified in the figure captions.

Simulations of all EPR and HYSCORE spectra were performed with the EasySpin program, a MATLAB toolbox developed for EPR simulations [12]. The HYSCORE data were processed with MATLAB 7.7.0 (The MathWorks, Inc., Natick, MA). The time traces were baseline corrected with a third-order polynomial, apodized with a Hamming window and zero filled. After a two-dimensional Fourier transformation, the absolute spectra were computed. Spectra recorded with different τ values were added after Fourier transformation to eliminate blind-spot effects.

3 Results and Discussions

Figure 2 shows the CW-EPR spectra of a frozen solution of imidazole-ligated *Ma*Pgb* at pH 8.5 at 5, 10 and 30 K. The spectrum can be decomposed into two

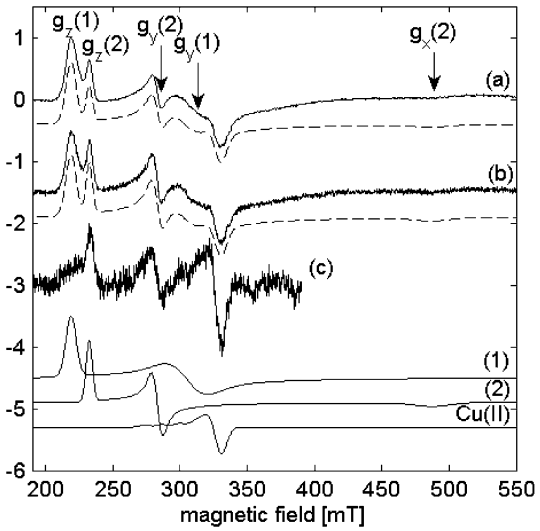

Fig. 2 X-band EPR spectra of a frozen solution of *Ma*Pgb* with a 10-fold excess of imidazole at pH 8.5 recorded at 5 K (**a**), 10 K (**b**) and 30 K (**c**). The *dashed lines* show the simulated spectra taking three components into account: low-spin ferric heme complexes (1) and (2) and a Cu(II) contaminant. These individual spectra used for the simulation are also shown

contributions typical of low-spin ferric heme systems [complexes (1) and (2)] and a Cu(II) complex. The latter is due to a Cu(II) contaminant from the chemicals used during protein purification and is of no importance for the further discussion. The two low-spin ferric heme complexes (1) and (2) have a different electronic relaxation behavior. While complex (2) can still be observed at temperatures around 50 K, complex (1) is not detectable above 30 K. This temperature dependence can be used to link the different spectral features to the two complexes (Fig. 2). Due to the large g strain, only the g_z and g_y principal values (low-field features) can be determined. While the broad dip around 490 mT may be due to the $g_x(2)$ feature, the $g_x(1)$ value cannot be derived from the CW-EPR spectra. This is a common problem encountered for low-spin ferric heme complexes with maximum g values higher than 3 [13]. In many cases, the lowest principal g value is derived from the over-simplified assumption that $\sum_i g_i^2 = 16$ [13]. However, the high-field features can be determined using ESE-detected EPR (Fig. 3). These experiments not only confirm the position of $g_x(2)$ (Fig. 3a), but allow to determine the position of the $g_x(1)$ feature at a magnetic field larger than 600 mT (Fig. 3b). The principal g values derived in this way are reported in Table 1. The relative amount of the two complexes at 5 K is 82% (±2%) for complex (1) and 18% (±2%) for complex (2).

It is interesting that contributions of two low-spin ferric heme complexes are observed in the EPR spectra of frozen ferric *Ma*Pgb*Im. The principal g values of these complexes differ significantly, but fall within the range of values typically observed for bis-imidazole-ligated ferric porphyrin complexes and heme proteins (Table 1). The values are typical for a $(d_{xy})^2(d_{xz}, d_{yz})^3$ ground state, with the g_z value pointing approximately along the heme normal [13]. The fact that g_z is larger than 3 and the high-field feature ($g = g_x$) is not observable with CW EPR, indicates that complex (1) of ferric *Ma*Pgb*Im is a so-called HALS (highly anisotropic low-spin)

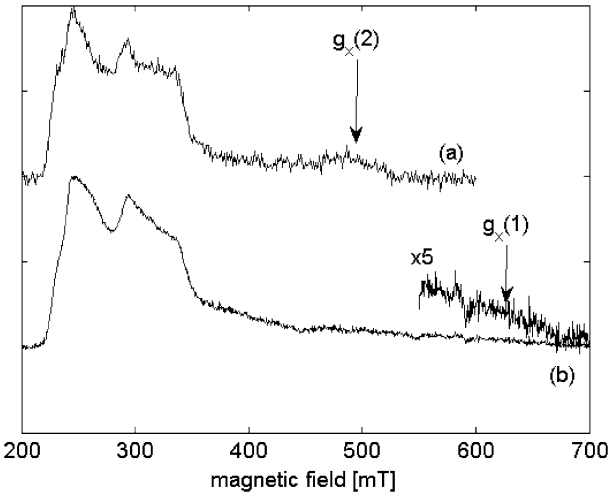

Fig. 3 ESE-detected spectra of a frozen solution of *Ma*Pgb* with a 10-fold excess of imidazole at pH 8.5 recorded at 4 K with **a** $\tau = 96$ ns, and **b** $\tau = 280$ ns

Table 1 Principal g values obtained from the simulation of the X-band CW-EPR and ESE-detected EPR spectra of frozen solutions of the imidazole-ligated *Ma*Pgb* compared to related systems reported in the literature

	g_z	g_y	g_x	V/λ	Δ/λ	References
*Ma*Pgb*Im Complex (1)	3.07 ± 0.01	2.17 ± 0.03	1.05 ± 0.04	1.27	2.30	This work
*Ma*Pgb*Im Complex (2)	2.90 ± 0.01	2.38 ± 0.01	1.38 ± 0.02	1.83	2.25	This work
hhMbIm	2.953 ± 0.01	2.25 ± 0.01	1.49 ± 0.01	1.82	3.26	This work
swMbIm	2.91	2.26	1.53	1.93	3.32	[14]
*Da*MbIm	2.99	2.26	1.51	1.81	3.37	[15]
CldIm	2.96	2.25	1.51	1.84	3.37	[16]
CytcIm	2.96	2.30	1.58	1.97	3.43	[17]
NP4-Im	3.02	2.25	1.46	1.72	3.24	[18]
[(OETPP)Fe(HIm)$_2$]Cl from	2.76	2.35	1.63	2.39	2.95	[19]
$CDCl_3$/cyclohexane	3.17	n.d.	n.d.			
[(OMTPP)Fe(1-MeIm)$_2$]Cl in	2.84	2.32	1.59	2.16	3.12	[20]
CD_2Cl_2	3.12	n.d.	n.d.			
[(TC_6TPP)Fe(1-MeIm)$_2$]Cl in	2.86	2.39	1.45	1.97	2.33	[20]
CD_2Cl_2	3.12	n.d.	n.d.			
$[PPIXFe(Im)_2]^+$	2.98	2.25	1.52	1.83	3.46	[21]
CYGB	3.20	2.08	1.20[a]	1.27	3.23	[22]

The corresponding ligand-field parameters are also given

DaMbIm imidazole-ligated ferric *Dolabella auricularia* Mb, *CldIm* imidazole-ligated chlorite dismutase, *cytcIm* imidazole-ligated cytochrome *c*, *NP4-Im* imidazole complex of *Rhodnius* nitrophorin NP4, *OETPP* octaethyltetraphenylporphyrin, *OMTPP* octamethyltetraphenylporphyrin, *PPIX* protoporphyrin, *1-MeIm* 1-methyl imidazole, *CYGB* human cytoglobin, *n.d.* not detected

[a] Predicted assuming $\sum_i g_i^2 = 16$, not experimentally detected

or type-I heme complex [13]. Complex (2) exhibits a much lower g anisotropy and can be classified as a 'regular' type-II heme center [13]. The x-ray diffraction structure of ferric *Ma*Pgb*Im revealed some heterogeneity in the heme region. In the majority of the molecules, the imidazole plane was oriented as shown in Fig. 1a, however, with a double configuration that involves a 180° flip of the imidazole plane [i.e. the imidazole nitrogen not bound to the Fe is either pointing towards the Tyr(B10)61 OH group or to the nitrogen atom of Trp(B9)60] [8]. Both states were equally occupied. In both states, the presence of the imidazole ligand induces a rotation of the Phe(E11)93 side chain around the C_β–C_γ bond of about 120° relative to the ligand-free *Ma*Pgb* [8]. In turn, this allows a rotation of Trp(B9)60 by 90° toward the heme center, thus closing one of the two apolar ligand-access tunnels in the protein. Although these are the predominant forms, some residual electron density was observed in the region where the Trp(B9)60 is located in the ligand-free *Ma*Pgb*, suggesting that, for a low percentage of the protein molecules in the crystal, the ligand-access tunnel is still open [8]. This may influence the orientation of the imidazole ligand.

The g-tensor of low-spin heme complexes is intimately related to the nature of the axial ligands to the iron, the relative orientation of these ligands, the binding

distances, and the distortions of the porphyrin ring, but the correlation is non-trivial [13, 20]. As shown by many authors [23–25], the *g*-tensor principal values can be linked to the ligand-field parameters V/λ and Δ/λ (V = rhombic splitting parameter, Δ = tetragonal splitting parameter, λ = spin-orbit coupling) (Table 1). From Table 1, it becomes clear that the principal *g* values and related ligand-field parameters of the imidazole complexes of Mbs, chlorite dismutase (Cld) and of the bis-imidazole complex of heme are very similar. Through a combination of different characterization techniques, it was shown that the latter *g* values agree with dihedral angles between the ligand imidazole planes in the order of 20°–30° [13, 21]. This indicates that the X-ray diffraction structure of the ferric swMbIm (Fig. 1b, [9]), in which a dihedral angle between the imidazole and proximal His plane of 47° is found, does not represent the situation in frozen solution. This may be due to the fact that the crystals were obtained by soaking the native ferric swMb crystals in solutions containing saturating levels of imidazole [9]. The crystal packing effects may have led to the formation of a more strained imidazole complex than the one formed in solution. In fact, an X-ray diffraction structure of the imidazole complex of blackfin tuna Mb recently deposited in the PDB bank (PDB structure 2QMA) reports a dihedral angle between the ligand planes of 24°.

The *g* anisotropy of NP4-Im is larger ($g_z = 3.02$) than the one found for the imidazole-ligated Mbs with a corresponding decrease in the V/λ value (Table 1), despite the fact that the dihedral angle between the two imidazole planes in NP4-Im is only 14° in the corresponding X-ray diffraction structure [18]. One of the big differences between this case and the former cases is the fact that the heme group is ruffled. This indicates that heme ruffling may influence the *g* anisotropy and rhombic splitting parameter of the ferric bis-imidazole-ligated hemes, although the effect seems relatively small. A far larger effect follows from a change in the dihedral angle between the two ligand planes. This is illustrated by the principal *g* values of ferric human cytoglobin (CYGB) [22], a globin having internal bis-histidine coordination of the heme iron, with a dihedral angle of 56° between the two imidazole planes of the histidines [26]. In this case, the V/λ value (1.27) is significantly lower than found for the imidazole-ligated Mbs and NP4-Im (1.7–1.95).

In all the above-mentioned cases, the Δ/λ values are about 3.2–3.5. However, complex (1) and (2) observed in the frozen solution of ferric *Ma*Pgb*Im have Δ/λ values of 2.25–2.3. A decrease in the tetragonal splitting has been related to an increase of the Fe–N_{axial} bond length because one of the ligands occupies a non-optimal position [20, 27]. It is at present unclear whether there can also be an influence of the ruffling on the tetragonal splitting.

The V/λ value of the dominant (HALS) complex (1) of ferric *Ma*Pgb*Im is the same as for ferric CYGB (Table 1), indicating that there will be a relatively large dihedral angle between the planes of the two axial ligands. The X-ray diffraction structure of *Ma*Pgb*Im reveals a dihedral angle between the planes of the external Im and His(F8)120 imidazole of $\sim$50° [8]. It seems therefore reasonable to assign complex (1) to the dominant conformation observed by X-ray diffraction.

The principal *g* values of complex (2) show a remarkably high g_y value in combination with a relatively small g_z value. The corresponding V/λ value is similar

to the one of the imidazole-ligated myoglobins, which have nearly parallel arrangement of the axial ligand planes. Interestingly, the EPR spectra of 1-methyl imidazole complexes of different iron porphyrins showed mixtures of two contributions, one characterized by a g_z value larger than 3 (a HALS species), and one with principal g values similar to those observed for complex (2) (Table 1, [20]). The latter contribution has been interpreted as stemming from a complex with nearly parallel orientation of the two imidazole planes [19, 20]. It thus seems that complex (2) agrees with a minority species with clearly different orientation of the exogenous imidazole ligand than the one depicted in Fig. 1a. The external

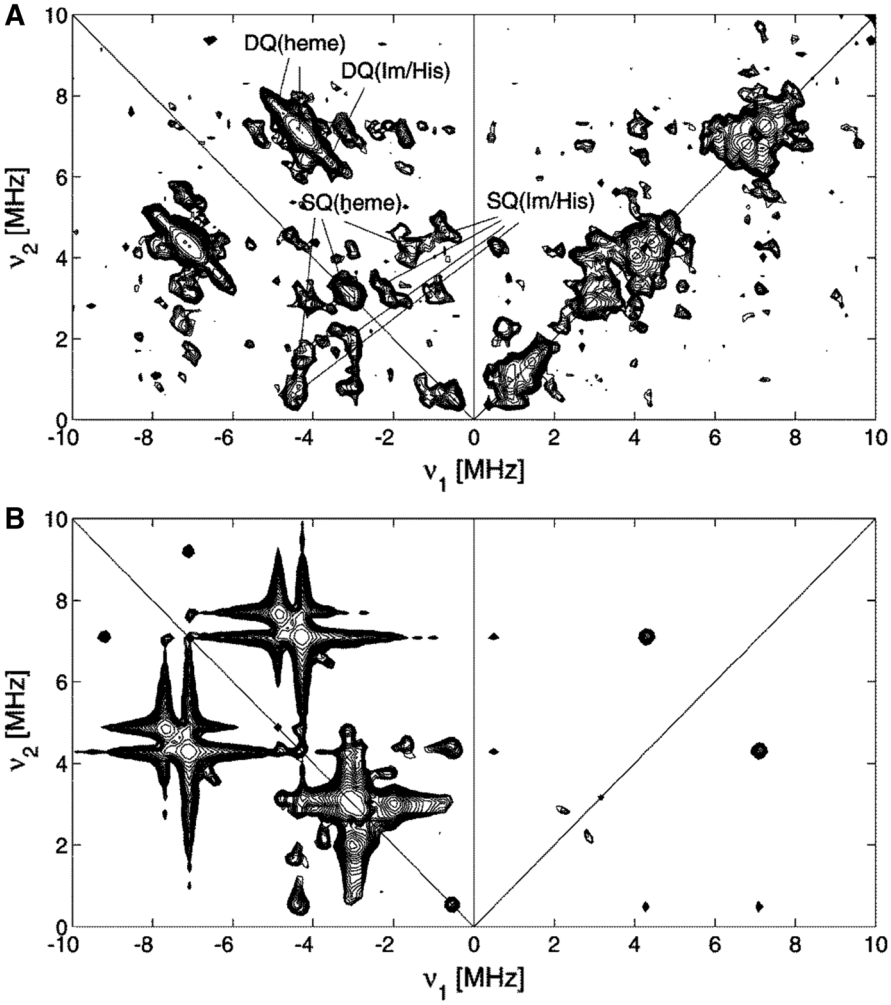

Fig. 4 **a** Experimental and **b** simulated ^{14}N HYSCORE spectrum of a frozen solution of ferric hhMbIm taken at an observer position agreeing with $g = g_z$ (236.2 mT). Both spectra are the sum of the HYSCORE spectra with $\tau = 96$ and 176 ns. The cross peaks linking the double-quantum (DQ) or the single-quantum (SQ) nuclear frequencies of the heme and Im or His ^{14}N nuclei are indicated

Table 2 Hyperfine (A_{zz}) and nuclear quadrupole (Q_{zz}, K) values determined at an observer position corresponding to $g = g_z$ for the imidazole-ligated globins under study in comparison to literature data

	^{14}N	$\lvert A_{zz}\rvert$ (MHz)	$\lvert Q_{zz}\rvert$ (MHz)	$\lvert K\rvert$ (MHz)	
hhMbIm	Heme (N1) (×2)	5.6 (±0.1)	0.5 (±0.1)	0.45 (±0.10)	This work
	Heme (N2) (×2)	6.2 (±0.1)	0.5 (±0.1)	0.45 (±0.10)	
	Im/His	5.0 (±0.1)	0.85 (±0.1)	0.43 (±0.05)	This work
swMbIm	Heme (N1) (×2)	5.8	0.46		[14]
	Heme (N2) (×2)	6.4	0.53		
	Im/His	5.7	n.d.		[14]
$[PPIXFe(Im)_2]^+$	Heme	5.9	0.42		[21]
	Im	5.2	0.85		[21]
CYGB	Heme	5.45	0.42		[29]
	His	5.0	0.9		[29]
*Ma*Pgb*Im (position $g_z(2)$)	Heme (N1) (×2)	5.4 (±0.1)	0.5 (±0.1)	0.45 (±0.10)	This work
	Heme (N2)	6.1 (±0.2)	0.5 (±0.1)	0.45 (±0.10)	
	Heme (N3)	6.6 (±0.2)	0.5 (±0.1)	0.45 (±0.10)	
	His	5.0 (± 0.2)	0.8 (±0.1)	0.40 (±0.05)	This work
	N4	3.7 (±0.2)	1.2 (±0.2)	0.6 (±0.1)	This work
*Ma*Pgb*Im (position $g_z(1)$)	Heme (N1)	5.4 (± 0.2)	0.5 (±0.2)	0.45 (±0.10)	This work
	Heme (N2)	6.1 (±0.2)	0.5 (±0.2)	0.45 (±0.10)	
	His	5.0 (±0.2)	0.8 (±0.1)	0.40 (±0.05)	This work

imidazole plane will be more parallel to the imidazole plane of the proximal His. This altered configuration may be related to a different orientation of the Trp(B9)60 residue as observed as a minority in the x-ray diffraction structure. Note that we can rule out the presence of bis-imidazole-ligated free heme due to protein denaturation, since the principal g values of this free heme complex are different from those of complex (2) (Table 1, [21]).

To further investigate the two EPR contributions found for ferric *Ma*Pgb*Im, HYSCORE experiments were undertaken. As a reference, the ^{14}N HYSCORE spectrum of a frozen solution of hhMbIm was recorded at the magnetic field position agreeing with g_z (236.2 mT) (Fig. 4a). The cross peaks linking the single-quantum (SQ) frequencies allow the determination of the hyperfine (A_{zz}) and nuclear quadrupole (Q_{zz}) components along the heme normal for the nitrogens bound to the iron. Further information on the nuclear quadrupole tensors can be obtained from the double-quantum (DQ) frequencies, that can be interpreted in terms of the hyperfine value (A_{zz}), the quadrupole coupling constant $K = e^2qQ/4h$, the asymmetry parameter η and the Larmor frequency ν_I via [28]

$$\nu_{\mathrm{DQ}}^{\alpha,\beta} = 2\sqrt{\left(\frac{A_{zz}}{2} \pm \nu_I\right)^2 + K^2(3+\eta^2)} \tag{1}$$

where K and η can be related to the quadrupole values in the usual way [28]. The largest component of the quadrupole tensor is equal to 2 K.

Using CW ENDOR, Scholes et al. [14] already showed that there is differing spin density on the heme nitrogens of ferric swMbIm [two sets of hyperfine/nuclear quadrupole values (Table 2)]. From isotope labeling experiments, they also derived that, at the g_z position, the ^{14}N hyperfine value of the coordinating nitrogen of the exogenous Im ligand should be below 5.7 MHz. The HYSCORE spectrum of ferric hhMbIm in Fig. 4a can be reproduced satisfyingly using hyperfine/nuclear quadrupole values that agree with those findings (Table 2; Fig. 4b). In the supplementary material, the simulated and experimental spectra are shown overlayed to allow a better comparison. Note that the simulations were performed

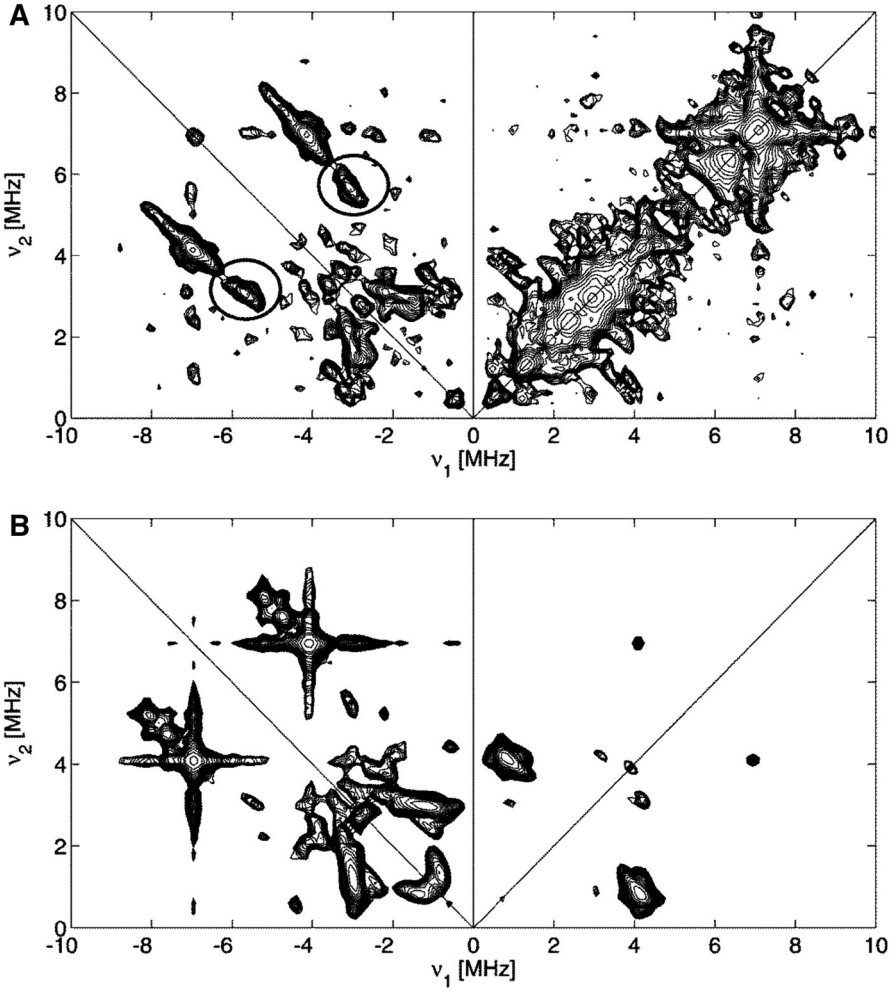

Fig. 5 **a** Experimental and **b** simulated ^{14}N HYSCORE spectrum of a frozen solution of ferric *Ma*Pgb*Im taken at an observer position agreeing with $g = g_z(2)$ (241.0 mT). Both spectra are the sum of the HYSCORE spectra with $\tau = 96$ and 280 ns. The unique set of cross peaks linking the double-quantum (DQ) nuclear frequencies of the N4 is *encircled*

assuming ideal pulses, which explains why the features on the diagonal of the (+, +) quadrant are not reproduced. Also, the simulations do not take strain effects of the hyperfine and nuclear quadrupole values into account. This will definitely be the case in reality (see also the large g strain in the CW-EPR spectra) and will lead to less sharp peaks in the experiment. The experimental HYSCORE spectrum is the result of the interaction of the unpaired electron with many nuclei. To reproduce the ^{14}N HYSCORE features, the interaction of the unpaired electron with (at least) the four nitrogens of the heme, one nitrogen of the exogenous Im and one of the F8His (i.e., a 7-spin system) should be taken into account. To reduce the computational times and taking advantage of symmetry, the simulated spectrum is taken as a four-spin system [$S = 1/2$ and $3 \times I = 1$ (the heme nitrogens N1, N2 and the imidazole nitrogen reported in Table 2)].

The above results can now be compared with the HYSCORE spectra of ferric *Ma*Pgb*Im taken at the magnetic field positions corresponding to $g = g_z(1)$ and $g = g_z(2)$ (see supplementary material for a systematic overlay of the spectra). While the HYSCORE spectrum taken at the magnetic field position agreeing with $g = g_z(1)$ will mainly reflect complex (1), the HYSCORE spectrum at $g = g_z(2)$ (Fig. 5a) will represent the contribution of both complexes due to the overlap of their corresponding EPR spectra (Fig. 2). From the overlay of the different HYSCORE spectra, it becomes clear that a unique set of cross peaks appears in the HYSCORE spectrum taken at $g = g_z(2)$ (indicated with circles in Fig. 5a). These cross peaks at (5.58, 3.05) MHz are not observed for observer position $g = g_z(1)$ or in the HYSCORE spectrum of ferric hhMbIm in Fig. 4b. The cross peak links the double-quantum (DQ) nuclear frequencies of a ^{14}N nucleus and can be related to the hyperfine and nuclear quadrupole parameters through Eq. (1). The extra set of cross peaks in Fig. 5a thus agrees with the following parameters: $|A_{zz}| \approx 3.7$ MHz, $0.53 \leq K \leq 0.61$ MHz for $1 \geq \eta \geq 0$. This A_{zz} hyperfine value is unusually low for bis-imidazole-ligated heme complexes (Table 2). Figure 5b shows a simulation of the HYSCORE spectrum of *Ma*Pgb*Im taken at $g = g_z(2)$ assuming the sum of two simulations: (1) a four-spin system including $S = 1/2$ and three heme ^{14}N nuclei (called N1, N2, and N3 in Table 2) and (2) a four-spin system with $S = 1/2$, and contributions typical for a heme ^{14}N nuclei (N1), a His nitrogen and the unusual ^{14}N contribution (indicated as N4 in Table 2). The overlay of the experimental and simulated spectrum is shown in the supplementary material. The agreement is satisfying, but not perfect. This may be due to the fact that both complexes (1) and (2) contribute to the HYSCORE spectrum at this position, leading to extra cross peaks due to complex (1).

Besides having different g values (Table 1), complexes (1) and (2) also seem to differ in the interactions between the unpaired electron and the iron-bound nitrogens. In the HYSCORE spectrum of *Ma*Pgb*Im taken at observer position $g = g_z(1)$, the contributions of N3 and N4 are missing (supplementary material). The higher variety in the heme nitrogen contribution (N1–N3) for complex (2) than for complex (1) may point to a change in the heme ruffling. The N4 contribution can be interpreted as stemming from an axial ligand. For imidazole complexes of ferric porphyrins, the largest nuclear quadrupole value is found to lie along the heme normal for the directly coordinated imidazole nitrogens, while this is in the heme

plane for the porphyrin nitrogens [21, 30]. The large Q_{zz} value of N4 thus indicates that this nucleus is part of an axial imidazole ligand. The Q_{zz} value of N4 agrees with an $|e^2qQ/h|$ value of 2.4 MHz, which is larger than the typical values found for His or Im nitrogens of other heme complexes (1.6–1.9 MHz) (Table 2), but smaller than the one of free imidazole (3.27 MHz [31]). Binding of a Lewis acid, such as a heme group, to imidazole leads to a lowering of the $|e^2qQ/h|$ value [32]. The fact that this effect is smaller than normal for the imidazole nitrogen N4 in complex (2) indicates a longer N–Fe bond in this case. This is corroborated by the smaller hyperfine value ($|A_{zz}|$) and also by the trend in the Δ/λ values as explained earlier (lowest Δ/λ value is found for complex (2) agreeing with a longer Fe–N distance). Hence, complex (2) agrees with a complex with quasi-parallel arrangement of the Im and His plane, but with a longer Fe–N_{Im} bond and possibly a different ruffling degree of the heme. Indeed, the higher variation in the hyperfine values of the heme nitrogens may point to a change in the porphyrin ruffling.

4 Conclusions

The CW-EPR spectra of a frozen solution of ferric MaPgb*Im reveal the presence of two heme complexes. The dominant contribution has g values and ^{14}N hyperfine/nuclear quadrupole contributions that agree with the heme configuration in the crystal structure of the imidazole complex of *Ma*Pgb* [8]. The minority complex indicates the presence of second conformer of the heme pocket, in which the imidazole plane is oriented parallel to the proximal His plane, and the Fe-N_{Im} bond is lengthened. The latter complex is probably associated with an orientation of the Trp(B9)60 residue as in the ligand-free *Ma*Pgb*, in which one of the ligand access tunnels is open [8].

Acknowledgments S. Van Doorslaer acknowledges the support from the Hercules Foundation, Flanders (Contract AUHA013). S. Van Doorslaer and S. Dewilde thank the Fund for Scientific Research–Flanders (FWO) for financial support (Grant G.0687.13).

References

1. S. Hou, T. Freitas, R.W. Larsen, M. Piatibratov, V. Sivozhelezov, A. Yamamoto, E.A. Melshkevitch, M. Zimmer, G.W. Ordal, M. Alam, Proc. Natl. Acad. Sci. USA **98**, 9353 (2001)
2. S.N. Vinogradov, D. Hoogewijs, X. Bailly, K. Mizuguchi, S. Dewilde, L. Moens, J.R. Vanfleteren, Gene **398**, 132 (2007)
3. T.A.K. Freitas, S. Hou, E.M. Dioum, J.A. Saito, J. Newhouse, G. Gonzalez, M.A. Gilles-Gonzalez, Proc. Natl. Acad. Sci. USA **101**, 6675 (2004)
4. T.A.K. Freitas, J.A. Saito, S. Hou, M. Alam, J. Inorg. Biochem. **99**, 23 (2004)
5. M. Nardini, A. Pesce, L. Thijs, J.A. Saito, S. Dewilde, M. Alam, P. Ascenzi, M. Coletta, C. Ciaccio, L. Moens, M. Bolognesi, EMBO Rep. **9**, 157 (2008)
6. J.E. Galagan, C. Nusbaum, A. Roy, M.G. Endrizzi, P. Macdonald, W. FitzHugh, S. Calvo, R. Engels, S. Smirnov, D. Anoor, A. Brown, N. Allen, J. Naylor, N. Stange-Thomann, J. Talamas, A. Tirrell, W. Ye, A. Zimmer, R.D. Barber, I. Cann, D.E. Graham, D.A. Grahame, A.M. Guss, R. Hedderich, C. Ingram-Smith, H.C. Kuettner, J.A. Krzycki, J.A. Leigh, W. Li, J. Liu, B. Mukhopadhyay, J.N. Reeve,

K. Smith, T.A. Springer, L.A. Umayam, O. White, R.H. White, E.C. de Macario, J.G. Ferry, K.F. Jarrell, H. Jing, A.J.L. Macario, I. Paulsen, M. Pritchett, K.R. Sowers, R.V. Swanson, S.H. Zinder, E. Lander, W.W. Metcalf, B. Birren, Genome Res. **12**, 532 (2002)
7. A. Pesce, L. Tilleman, S. Dewilde, P. Ascenzi, M. Coletta, C. Ciaccio, L. Moens, M. Bolognesi, M. Nardini, IUBMB Life **63**, 287 (2011)
8. A. Pesce, L. Tilleman, J. Donné, E. Aste, P. Ascenzi, C. Ciaccio, M. Coletta, L. Moens, C. Viappiani, S. Dewilde, M. Bolognesi, M. Nardini, PLoS One **8**, e66144 (2013)
9. C. Lionetti, M.G. Guanziroli, F. Frigerio, P. Ascenzi, M. Bolognesi, J. Mol. Biol. **217**, 409 (1991)
10. S. Van Doorslaer, L. Tilleman, B. Verrept, F. Desmet, S. Maurelli, F. Trandafir, L. Moens, S. Dewilde, Inorg. Chem. **51**, 8834 (2012)
11. P. Höfer, A. Grupp, H. Nebenführ, M. Mehring, Chem. Phys. Lett. **132**, 279 (1986)
12. S. Stoll, A. Schweiger, J. Magn. Reson. **178**, 42 (2006)
13. F.A. Walker, Coord. Chem. Rev. **185–186**, 471–534 (1999)
14. C.P. Scholes, K.M. Falkowski, S. Chen, J. Bank, J. Am. Chem. Soc. **108**, 1660 (1986)
15. Y. Yamamoto, T. Suzuki, H. Hori, Biochim. Biophys. Acta **1248**, 149 (1995)
16. P.L. Hagedoorn, D.C. de Geus, W.R. Hagen, Eur. J. Biochem. **269**, 4905 (2002)
17. M. Ikeda-Saito, T. Iizuka, Biochim. Biophys. Acta **393**, 335 (1975)
18. R.E. Berry, X.D. Ding, TKh Shokhireva, A. Weichsel, W.R. Montfort, F.A. Walker, J. Biol. Inorg. Chem. **9**, 135 (2004)
19. L.A. Yatsunyk, A. Dawson, M.D. Carducci, G.S. Nichol, F.A. Walker, Inorg. Chem. **45**, 5417 (2006)
20. L.A. Yatsunyk, M.D. Carducci, F.A. Walker, J. Am. Chem. Soc. **125**, 15986 (2003)
21. I. García-Rubio, G. Mitrikas, J. Biol. Inog. Chem. **15**, 929 (2010)
22. E. Vinck, S. Van Doorslaer, S. Dewilde, L. Moens, J. Am. Chem. Soc. **126**, 4516 (2004)
23. J.S. Griffith, Nature **180**, 30 (1957)
24. C.P.S. Taylor, Biochim. Biophys. Acta **491**, 137 (1977)
25. P.J. Alonso, J.I. Martínez, I. García-Rubio, Coord. Chem. Rev. **251**, 12 (2007)
26. H. Sugimoto, M. Makino, H. Sawai, N. Kawada, K. Yosizato, Y.J. Shiro, Mol. Biol. **339**, 873 (2004)
27. R. Quinn, J. Selverstone Valentine, M.P. Byrn, C.E. Strouse, J. Am. Chem. Soc. **109**, 3301 (1987)
28. S.A. Dikanov, Yu. Tsvetkov, M.K. Bowman, A. Astashkin, Chem. Phys. Lett. **90**, 149 (1982)
29. A.I. Ioanitescu, S. Van Doorslaer, S. Dewilde, B. Endeward, L. Moens, Mol. Phys. **105**, 2073 (2007)
30. E. Vinck, S. Van Doorslaer, Phys. Chem. Chem. Phys. **6**, 5324 (2004)
31. M.J. Hunt, A.L. MacKay, D.T. Edmonds, Chem. Phys. Lett. **34**, 473 (1975)
32. Y.-N. Hsieh, G.V. Rubenacker, C.P. Cheng, T.L. Brown, J. Am. Chem. Soc. **99**, 1384 (1977)